On the Interaction of Grazing Acoustic Waves and Turbulent Boundary Layer over Acoustic Liners

DOI: 10.61782/fa.2025.0650

FORUM ACUSTICUM EURONOISE 2025

ON THE INTERACTION OF GRAZING ACOUSTIC WAVES AND TURBULENT BOUNDARY LAYER OVER ACOUSTIC LINERS

Angelo Paduano[1*] **Francesco Scarano**[1] **Damiano Casalino**[2]
Julio Cordioli[3] **Francesco Avallone**[1]
[1]Department of Mechanical and Aerospace Engineering, Politecnico di Torino, Torino, Italy
[2] Flow Physics and Technology, Delft University of Technology, Delft, Netherlands
[3]Department of Mechanical Engineering, Federal University of Santa Catarina, Florianópolis, Brazil

ABSTRACT

Acoustic liners, passive devices to mitigate engine noise, operate under high-speed grazing flow and grazing acoustic waves. To investigate the complex physics governing this interaction, high-fidelity numerical simulations of a spatially evolving turbulent boundary layer grazing a multi-orifice acoustic liner at a bulk Mach number of 0.32 are performed. The simulations replicate conditions from a reference experiment. Grazing tonal plane acoustic waves with amplitudes of 130 dB and 145 dB and propagating in the same direction and the direction opposite to the mean flow are analyzed. The results show that the boundary layer displacement thickness doubles in the presence of the liner and its growth rate is affected by the amplitude and propagation direction of the acoustic wave. The acoustic liner also promotes the formation of an outer hump in both the logarithmic region of the streamwise and wall-normal velocity variance, with these effects becoming more pronounced under acoustic forcing. Furthermore, impedance estimation, using Dean's method, reveals that near-wall flow modifications, quantified through the displacement thickness, influence the local value of the computed impedance.

Keywords: *aeroacustics, acoustic liners, impedance, semi-empirical model.*

**Corresponding author*: *angelo.paduano@polito.it.*

1. INTRODUCTION

Acoustic liners are essential components to reduce noise in aircraft engines. They are typically installed in the intake and core jet sections of aircraft engines. The advent of ultra-high bypass ratio engines, characterized by larger fan diameters, has significantly increased the contribution of fan noise, comprising a tonal component at the Blade-Passing Frequency (BPF) and broadband noise due to rotor-stator turbulence interaction [1–3].

Acoustic liners vary in complexity and absorption properties. Conventional Single Degree-Of-Freedom (SDOF) liners consist of a perforated face sheet, a backing cavity, and a rigid backplate, operating as Helmholtz resonators tuned to the fan's BPF or harmonics [4]. A widely used approach to characterize the acoustic liner is to measure its acoustic impedance, a quantity defined in the frequency domain as:

$$\hat{Z}(\omega) = \frac{\hat{p}}{\hat{v} \cdot \mathbf{n}} = \theta + i\chi, \tag{1}$$

where p is the acoustic pressure, u_n the acoustic particle velocity normal to the face sheet, θ the resistance, and χ the reactance. Although impedance is an intrinsic property of the liner surface, studies have shown that it is highly sensitive to the eduction technique used for its calculation [5]. Furthermore, impedance is strongly influenced by the presence of grazing flow, with research highlighting its dependence on boundary layer parameters, particularly the displacement thickness δ^* [6].

The presence of a grazing flow adds complexity to impedance eduction, requiring an appropriate boundary condition. The most widely adopted boundary condition is the Ingard-Myers one [7], which assumes an in-

finitely thin vortex sheet along the liner surface. To improve accuracy, several studies have incorporated boundary layer profiles with finite thickness in impedance modeling [8–10]. To characterize the flow near the wall, fully three-dimensional numerical simulations of sound interacting with laminar and turbulent boundary layers were performed by Zhang and Bodony [11]. Although this computational study provided valuable information on flow-acoustic interactions within a single orifice, it remained limited to single-resonator configurations and did not account for boundary layer modifications induced by multiple cavities.

A step forward was taken by Shahzad et al. [12], who performed pore-resolved compressible direct numerical simulations of a turbulent flow that grazes a multi-cavity acoustic liner. Their findings show that the turbulent flow over an acoustic liner behaves similarly to flow over a porous surface. However, their study did not consider the presence of acoustic waves.

A comprehensive analysis of the acoustic and aerodynamic fields over multi-cavity liners, particularly the boundary layer evolution and its effect on impedance, remains lacking. This study employs high-fidelity numerical simulations using the Lattice-Boltzmann Very-Large-Eddy-Simulation (LB/VLES) approach to model a turbulent boundary layer grazing an acoustic liner in the presence of grazing acoustic waves. The simulated geometry corresponds to the one experimentally investigated by Bonomo et al. [6].

The paper is structured as follows: section 2 details the methodology and the computational setup. Section 3 presents and discusses the numerical results. Section 4 summarizes the main findings.

2. METHODOLOGY

2.1 Solver

The commercial software 3DS Simulia PowerFLOW version 6 is adopted. It is based on an extended LB method. A VLES approach is used, which resolves only the large turbulent scales. It accounts for sub-grid effects using a turbulence model based on two-equation renormalization group theory k-ϵ. This approach differs from the computation of an equivalent eddy viscosity. It dynamically adjusts the Boltzmann model to match the characteristic time scales of turbulent flow. Reynolds stresses are not explicitly added to the governing equations; they arise implicitly from the chaotic exchange of momentum in turbulent flow, where characteristic times are shorter than the slowly varying turbulent flow.

To reduce the computational approach, a wall-model based on the extended law-of-the-wall is adopted [13]. This solver has been widely used to study fluid dynamic and aeroacoustic fields over acoustic liners [14–16].

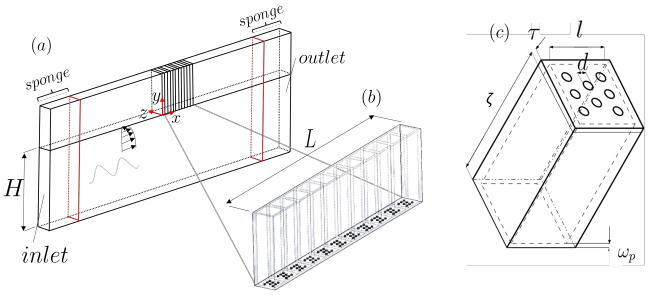

Figure 1: Overview of the computational domain: (a) schematic of the simulation setup, (b) detailed view of the acoustic liner, and (c) magnified depiction of a single cavity.

2.2 Numerical set-up

The computational domain, shown in Fig. 1, replicates the UFSC grazing flow test facility [17]. The liner is positioned on the top wall of a channel with rectangular cross section. The channel height is $H = 2h = 40$ mm. Each cavity, with a square cross-section $l = 8.46d$ and depth $\zeta = 32.56d$ ($d = 1.17$ mm is the orifice diameter), has eight orifices, partition walls with thickness $w_p = 2.17d$, and a face sheet $\tau = 0.46d$ thick. This configuration results in a cavity porosity of 5.63%. The simulated liner consisted of a row of eleven cavities, yielding a total streamwise length of $L = 116.23d$. A zig-zag trip with a height of $0.21d$ and length of $1.71d$ is placed upstream at $x = -1367d$ to match the experimental velocity profile [17].

The simulation is initialized with the flow at rest. A inflow velocity boundary condition is applied at the inlet, allowing the flow to develop spatially within the channel until statistical convergence is reached. For the acoustic simulations, an instantaneous flow field is saved and modified by superimposing a plane acoustic wave with a specified frequency and amplitude using the *OptydB* toolkit. This modified flow field serves as the initial condition for the simulations that include the acoustic excitation.

A total of five cases are tested, as summarized in Table 1. The first case is the smooth wall one; it serves as the baseline reference. The second case has a lined wall subjected to the same turbulent boundary layer. In the remaining cases, acoustic excitation is added at a fixed frequency of 1400 Hz, with SPLs equal to 130 dB and 145 dB. For both SPLs, cases with upstream and downstream acoustic wave propagation are tested. However, since the 130 dB cases exhibited trends similar to those at 145 dB, only the latter are presented for brevity.

2.3 In-situ technique

In this work, impedance is computed using the in-situ technique proposed by Dean [18]. It involves measuring unsteady pressure at the face sheet and the bottom of the cavity. This method provides a local measurement of impedance. It is based on the following key assumptions: the wavelength of the incident acoustic wave is significantly larger than the cavity width; the walls of the cavity are considered to be sufficiently thick, resulting in the liner being locally reactive; any wave entering the cavity is assumed to be completely reflected at the backplate. Consequently, the acoustic pressure of the standing wave within the cavity is the sum of the incident and reflected waves. Using the linearized momentum equation, it is possible to calculate the acoustic-induced velocity and, subsequently, the impedance as:

$$Z_f = \frac{Z}{Z_0} = -i\tilde{H}_{fb}\frac{1}{\sin(k\lambda)}; \qquad (2)$$

where Z_0 is the characteristic impedance of air, $\tilde{H}_{fb}$ is the transfer function defined as the ratio between the pressure measured at the face sheet $\tilde{p}_f$ and at the backplate $\tilde{p}_b$, and $k = \omega/c_0$ is the free-field wavenumber, with ω being the acoustic wave angular frequency. This technique has been widely used for calculating the impedance of acoustic liners in the presence of grazing flow [11, 19]. Unlike impedance eduction techniques [17], a model of the acoustic field is not required for the in-situ technique, so boundary conditions to model the presence effects of the boundary layer are unnecessary. However, studies have underlined the sensitivity of this technique on the sampling position [20, 21].

Mach	Case	SPL (dB)	Freq. kHz	ac. pos.
0.32	Smooth	-	-	-
0.32	Lined	-	-	-
0.32	Lined	130	1.4	up
0.32	Lined	145	1.4	up
0.32	Lined	145	1.4	down.

Table 1: List of simulations carried out.

3. RESULTS

3.1 Mean flow velocity profiles

Figure 2 presents streamwise velocity profiles sampled at three locations along the liner: $x/L = 0$, $x/L = 0.5$ and $x/L = 1$. The velocity profiles are expressed in outer coordinates, where U_∞ denotes the centerline streamwise velocity, and h is the half height of the channel.

Figure 2a compares the mean velocity profiles with and without the liner and in the absence of grazing acoustic wave. It can be observed that introducing a liner causes a velocity shift. Figure 2b compares the velocity profiles at $x/L = 0$ and $x/L = 0.5$ in the absence of acoustic excitation. The presence of cavities affects the near-wall flow, with a further velocity shift of $\Delta U = -14\%$ in the range $0.01 < y/h < 0.04$ at $x/L = 0.5$ compared to $x/L = 0$. Conversely, comparing the velocity profiles at $x/L = 1$ with the one at $x/L = 0.5$ (Figure 2c) it can be observed that the velocity shift is reduced to $\Delta U = -3\%$.

The effect of the presence of the acoustic wave is visible already upstream of the lined section. As a matter of fact, a slight downward shift in velocity compared to the no-acoustic case, $\Delta U = -4\%$, is found in the region $0.01 < y/h < 0.04$ for the upstream propagating wave with SPL equal to 145dB. At $x/L = 0.5$, the influence of acoustic waves is more pronounced than in the upstream region. As shown in Figure 2e, a higher SPL increases the velocity deficit. As a matter of fact, for the cases with SPL = 130 dB the differences with respect to the no-acoustic cases are smaller ($\Delta U = -4\%$) than for the cases with higher SPL ($\Delta U = -8\%$). At the end of the liner ($x/L = 1$, Figure 2f) the differences between acoustically excited cases and the no-acoustic case are within 3%.

The comparison of the velocity profiles between upstream and downstream propagating wave shows that the largest difference appears at $x/L = 0.5$ (Figure 2h); the downstream case exhibits a velocity profile closer to the no-acoustic case, with deviations remaining below -4%. Furthermore, downstream of the liner, the combined effect of the cavities and grazing acoustic waves diminishes.

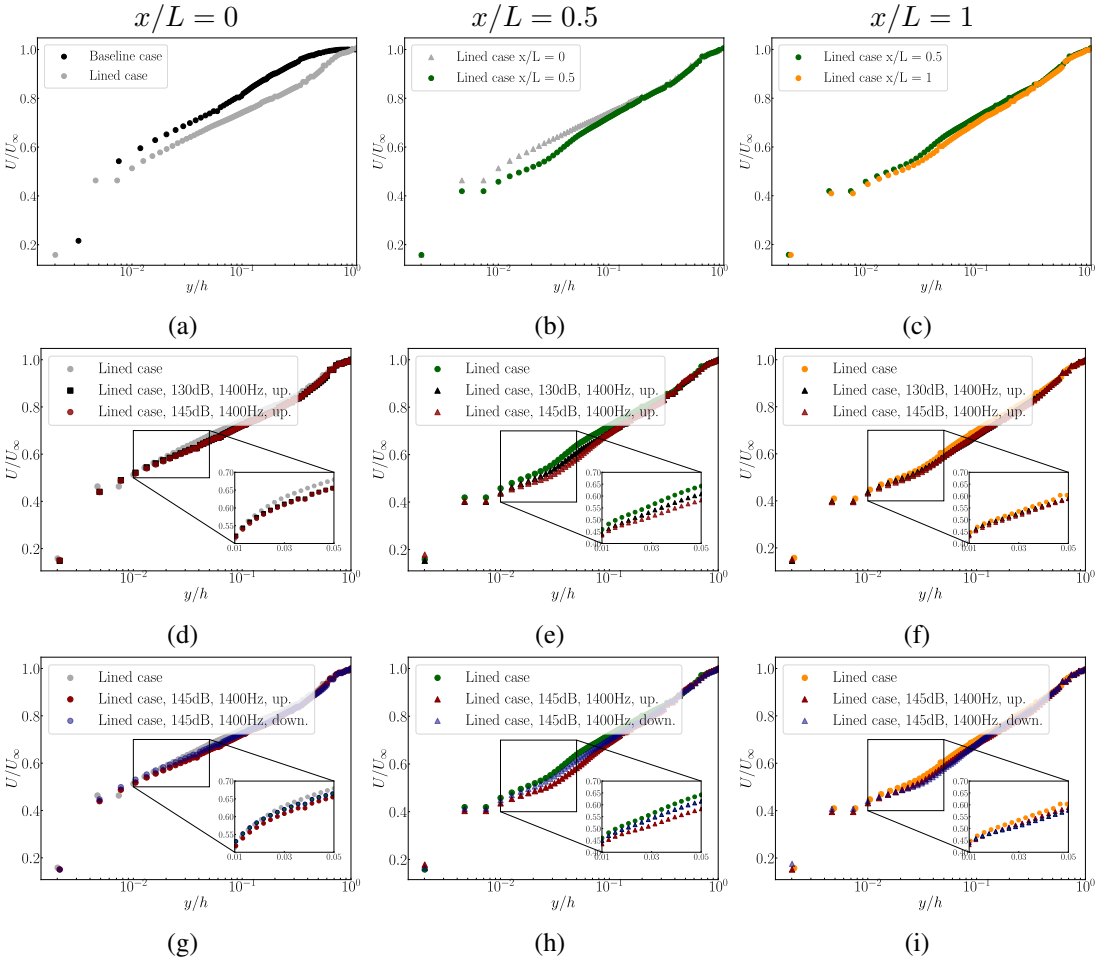

Figure 2: Streamwise velocity profiles in outer coordinates at three different locations along the liner: (left column) $x/L = 0$, (center column) $x/L = 0.5$, and (right column) $x/L = 1$. Velocity profiles are normalized by the centerline velocity U_∞ and channel half-height.

3.2 Integral boundary layer parameter streamwise evolution

Although these parameters are not commonly used for turbulent channel flows, some, such as δ^*, are present in the semi-empirical model for predicting impedance .

In this context, the boundary layer displacement thickness δ^* is defined as:

$$\delta^* = \int_0^h \left(1 - \frac{U(y)}{U_\infty}\right) dy \tag{3}$$

Figure 3 shows that, in the presence of the liner, δ^* increases by approximately 50% with respect to the smooth wall case. δ^* shows localized humps after each orifice, followed by a slight decrease until the next pair of orifices is encountered. This periodic variation results in an overall displacement thickness increase of 13% at the end of the liner.

The streamwise development of δ^* is also dependent on the presence of the acoustic wave, its amplitude and direction of propagation. As shown in Figure 3a, the presence of the acoustic wave increases the δ^*; starting from $x/L = 0.5$ the impact of the SPL also is visible even if it is not very strong. On the other hand, differences become more relevant when assessing the impact of the direction of propagation of the acoustic wave: the case

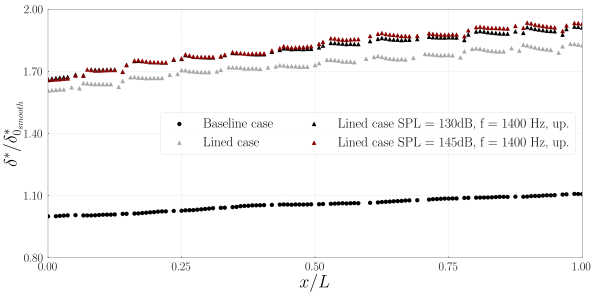

(a)

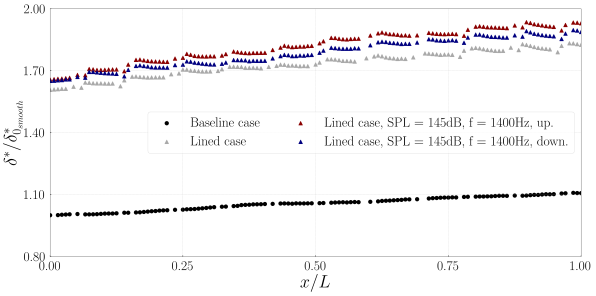

(b)

Figure 3: Streamwise evolution of δ^* over the liner: (a) effect of different sound pressure levels at a fixed frequency of 1400 Hz, (b) effect of acoustic wave propagation direction at SPL = 145 dB.

with a downstream-propagating wave exhibits a slightly lower increase in δ^* compared to the upstream propagating case. Nonetheless, differences in boundary layer displacement thickness remain below 5% relative to the no-acoustic case, whereas the most significant effect is the 50% increase in δ^* caused by the presence of the liner and the oscillatory variations over the cavities. These findings highlight that the presence of the lined surface is the most important factor that affects the boundary layer development.

3.3 Variance of the velocity fluctuations

The variance of streamwise and wall-normal velocity fluctuations normalized by the centerline velocity are reported in Figure 4. The variance profiles are sampled at three different streamwise locations: $x/L = 0$, $x/L = 0.5$ and $x/L = 1$.

Upstream of the liner, profiles of both the streamwise and wall-normal velocity variance collapse, closely resembling the one obtained for the smooth wall. At $x/L = 0.5$, an outer hump emerges in the variance of the streamwise velocity component for the no-acoustic case. This indicates that the lined surface alters the distribution and amplitude of the velocity fluctuations within the boundary layer. A clear secondary peak in streamwise velocity turbulent fluctuations appears at $y/h \approx 0.1$. At the same location, also the fluctuations of the wall-normal velocity component show an increase. These findings align with previous results on porous material [22, 23] and are likely related to a development of secondary flow structures, due to the injection of momentum near the wall [24]. The intensity of both peaks increases at downstream locations (i.e., $x/L = 1$), with the vertical velocity component showing a larger increase than the wall-parallel one.

It is interesting to note that the introduction of acoustic excitation modifies the turbulence statistics. The outer hump is more pronounced as the SPL increases. This is demonstrated by comparing Figure 4 (b) and (c). At the most downstream location $x/L = 1$, the amplitude of the acoustic source is higher for the downstream acoustic source because the acoustic amplitude is higher. Furthermore, it is also possible to notice that the development of the flow has also an impact on the wall-normal profile of the variance of the streamwise velocity fluctuations. At the most downstream location, a higher amplitude of the acoustic wave shows a more uniform high-intensity fluctuations region with a less evident difference between the inner and outer peaks. Conversely, the wall-normal velocity fluctuations show less dependence on the intensity of the acoustic source with the peak at $x/L = 1$ being very similar.

3.4 Impedance streamwise analysis

Using the in-situ technique on a numerical database, it is possible to analyze the distribution of impedance on the entire liner surface, thus providing insights into how individual orifices affect locally the impedance value.

Figures 5 show the distribution of resistance and reactance values computed on all the streamwise points at $z/l = 0.5$. A periodic pattern emerges in the distribution of resistance for all cases, with values doubling along each cavity peaking after the orifices and tending to decrease near the end of the cavity. This pattern follows the one discussed for δ^* (Figure 3). This is observed regardless of SPL value and the acoustic wave propagation direction; however, the downstream case shows higher variation of resistance compared to the upstream one. Considering the

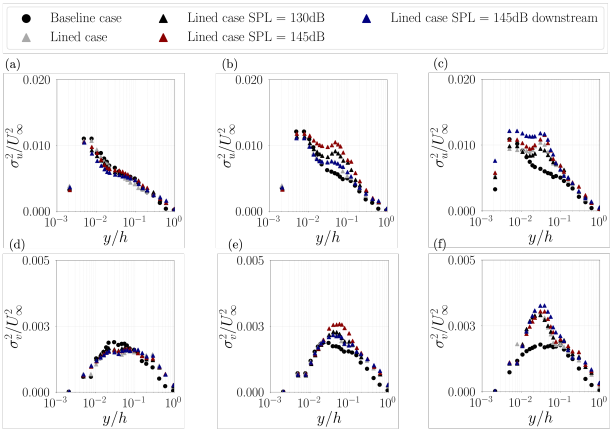

Figure 4: Streamwise (top row) and wall-normal (bottom row) velocity variance at three streamwise locations: $x/L = 0$ (a-d), $x/L = 0.5$ (b-e), and $x/L = 1$ (c-f).

variation of resistance along each cavity, this is enhanced for the downstream propagating case.

Considering the mean resistance value, small differences are found between the cases analyzed. The upstream acoustic source case yields $\theta = 0.78$ for SPL = 130 dB and $\theta = 0.80$ for SPL = 145 dB, while for the downstream case at SPL = 145 dB $\theta = 0.82$.

Reactance exhibits spatial variations across each cavity, following a trend that depends on the propagation direction of the acoustic wave. This is consistent with the established relationship between reactance and the phase of the acoustic wave. In the downstream acoustic source case, reactance variation is reduced compared to the upstream case. However, as for the resistance, the differences in the mean values are not large. Specifically, for SPL = 130 dB the mean reactance is $\chi = -0.52$, while, for SPL = 145 dB, the upstream acoustic source case yields $\chi = -0.46$ and the downstream case $\chi = -0.47$. Previous studies employing in-situ measurement techniques [16] have reported similar spatial dependencies in resistance and reactance within a single cavity.

These findings indicate that the wake generated by each orifice has a relevant impact on the impedance computed with the Dean's method.

To evaluate the impact of the local boundary layer profiles, Figure 5 compares the computed components of impedance with the one predicted by a semi-empirical model [25]. This model requires as input the value of δ^*. In this case, the prediction obtained using the δ^* from the smooth-wall simulation upstream of the liner, as it is typically done, and the prediction obtained using the δ^* obtained at each streamwise location in the presence of the liner. Results obtained with the latter agree better with the simulation results, regardless of the acoustic wave propagation direction. When the smooth-wall displacement thickness is used in the semi-empirical model, the discrepancy in impedance estimation is 17%, whereas incorporating the local boundary layer displacement thickness it reduces to 3%. Similar results are found for the reactance.

4. CONCLUSION

This study investigates the interaction between grazing acoustic waves and a turbulent boundary layer over an acoustic liner using high-fidelity numerical simulations. The study revealed that the presence of the liner leads to a 50% increase in displacement thickness (δ^*) compared to a smooth wall, with an additional 13% streamwise growth. The downstream-propagating wave results in a slightly lower δ^* growth compared to the upstream case. Overall, the impact of acoustic waves remains secondary to that of the cavities. This confirms that the liner geometry plays a dominant role in modifying the boundary layer, with the impact of acoustic forcing diminishing towards the liner's downstream end. The lined surface alters second-order flow statistics, promoting the formation of an outer hump in the streamwise and wall-normal velocity variance. This effect is amplified by acoustic forcing, particularly at higher SPLs, causing an increased inner-outer interaction within the boundary layer. The modifications in the grazing flow streamwise evolution have been linked to impedance through in-situ eduction technique. The impedance eduction analysis reveals significant spatial variations in resistance and reactance. The periodic pattern in resistance, peaking just after each orifice and decreasing within the cavity, closely follows the displacement thickness evolution. The study highlights that assuming a uniform boundary layer profile different from the local one leads to inaccuracies in impedance predictions, particularly when using semi-empirical models. The direction of acoustic wave propagation affects both flow statistics and impedance characteristics. However, differences in mean resistance and reactance values remain minimal, reinforcing the idea that local variations play a more significant role than acoustic propagation direction.

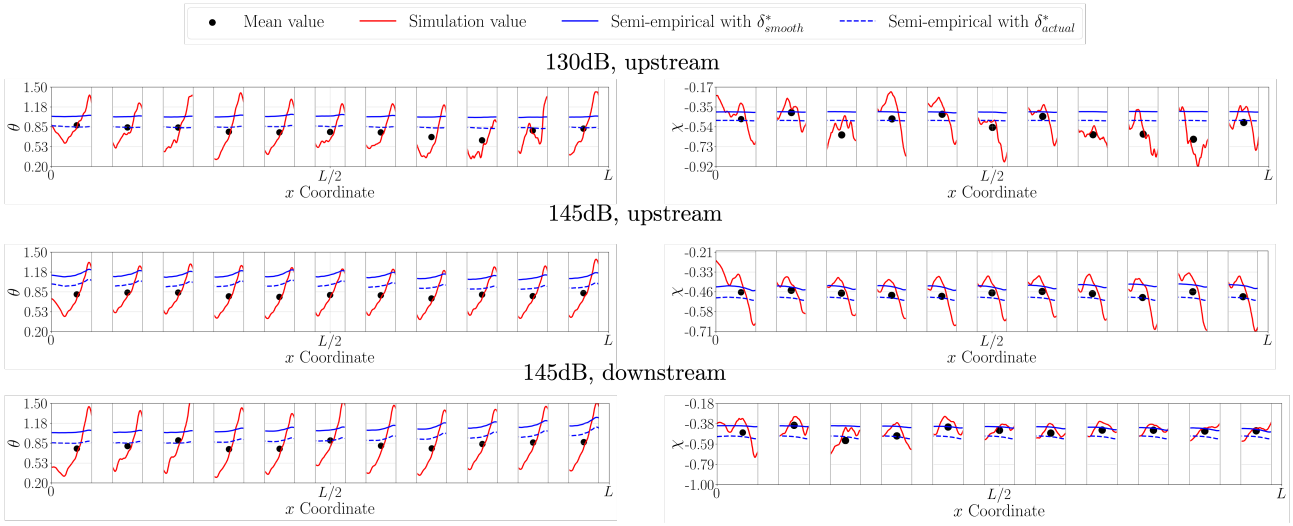

Figure 5: Streamwise distribution of (left) resistance, and (right) reactance along the liner surface for different acoustic wave's SPLs and direction of propagation at fixed $f = 1400$ Hz.

5. ACKNOWLEDGMENTS

The work of A. Paduano and F. Avallone is co-funded by the European Union (ERC, LINING, 101075903). Views and opinions expressed are however those of the author(s) only and do not necessarily reflect those of the European Union or the European Research Council. Neither the European Union nor the granting authority can be held responsible for them. This work was partially supported by the AeroAcoustics Research Consortium (AARC). The AARC is a government-industry partnership supporting pre-competitive research for aircraft noise reduction. J.A. Cordioli gratefully acknowledge funding from Conselho Nacional de Desenvolvimento Científico e Tecnológico (CNPq), project number 407583/2022-0.

6. REFERENCES

[1] S. Mallat, "A theory for multiresolution signal decomposition: the wavelet representation," *IEEE Transactions on Pattern Analysis and Machine Intelligence*, vol. 11, no. 7, pp. 674–693, 1989.

[2] C. Hughes, "The Promise and Challenges of Ultra High Bypass Ratio Engine Technology and Integration," *AIAA Aero Sciences Meeting*, pp. 0–11, 2011.

[3] D. Casalino, A. Hazir, and A. Mann, "Turbofan broadband noise prediction using the lattice boltzmann method," *AIAA Journal*, vol. 56, no. 2, 2018.

[4] R. E. Motsinger and R. E. Kraft, "4 Design and Performance of Duct Acoustic Treatment," in *NASA. Langley Research Center, Aeroacoustics of Flight Vehicles: Theory and Practice. Volume 2: Noise Control*, 1991.

[5] F. Avallone, A. Paduano, L. M. Pereira, L. A. Bonomo, J. A. Cordioli, D. Casalino, and D. Cerizza, "On the comparison of different methods for impedance eduction applied to a numerical database," in *30th AIAA/CEAS Aeroacoustics Conference (2024)*, 2024.

[6] L. A. Bonomo, N. Quintino, J. A. Cordioli, F. Avallone, M. G. Jones, B. M. Howerton, and D. M. Nark, "A Comparison of Impedance Eduction Test Rigs with Different Flow Profiles," in *AIAA AVIATION 2023 Forum*, 2023.

[7] U. Ingård and S. Labate, "Acoustic circulation effects and the nonlinear impedance of orifices," *The Journal of the Acoustical Society of America*, vol. 22, pp. 211–218, 03 1950.

[8] E. J. Brambley, "Well-posed boundary condition for acoustic liners in straight ducts with flow," *AIAA Journal*, vol. 49, no. 6, pp. 1272–1282, 2011.

[9] S. W. Rienstra and M. Darau, "Boundary-layer thickness effects of the hydrodynamic instability along an impedance wall," *Journal of Fluid Mechanics*, vol. 671, p. 559–573, 2011.

[10] Y. Aurégan, R. Starobinski, and V. Pagneux, "Influence of grazing flow and dissipation effects on the acoustic boundary conditions at a lined wall," *The Journal of the Acoustical Society of America*, vol. 109, no. 1, 2001.

[11] Q. Zhang and D. J. Bodony, "Numerical investigation of a honeycomb liner grazed by laminar and turbulent boundary layers," *Journal of Fluid Mechanics*, vol. 792, pp. 936–980, 3 2016.

[12] H. Shahzad, S. Hickel, and D. Modesti, "Turbulence and added drag over acoustic liners," *Journal of Fluid Mechanics*, vol. 965, 6 2023.

[13] B. E. Launder and D. B. Spalding, "The numerical computation of turbulent flows," *Computer Methods in Applied Mechanics and Engineering*, vol. 3, no. 2, 1974.

[14] A. Hazir and D. Casalino, "Effect of temperature variations on the acoustic properties of engine liners," in *23rd AIAA/CEAS Aeroacoustics Conference, 2017*, 2017.

[15] A. Mann, F. Pérot, M. S. Kim, and D. Casalino, "Characterization of acoustic liners absorption using a lattice-Boltzmann method," in *19th AIAA/CEAS Aeroacoustics Conference*, 2013.

[16] F. Avallone, P. Manjunath, D. Ragni, and D. Casalino, "Lattice-boltzmann very large eddy simulation of a multi-orifice acoustic liner with turbulent grazing flow," in *25th AIAA/CEAS Aeroacoustics Conference, 2019*, 2019.

[17] L. A. Bonomo, N. T. Quintino, A. M. Spillere, J. A. Cordioli, and P. B. Murray, "A Comparison of In-Situ and Impedance Eduction Experimental Techniques for Acoustic Liners with Grazing Flow and High SPL," in *28th AIAA/CEAS Aeroacoustics Conference, 2022*, 2022.

[18] P. Dean, "An in situ method of wall acoustic impedance measurement in flow ducts," *Journal of Sound and Vibration*, vol. 34, no. 1, pp. 97–IN6, 1974.

[19] B. Schuster, "A comparison of ensemble averaging methods using Dean's method for in-situ impedance measurements," in *18th AIAA/CEAS Aeroacoustics Conference (33rd AIAA Aeroacoustics Conference)*, 2012.

[20] L. M. Pereira, L. A. Bonomo, N. T. Quintino, A. R. da Silva, J. A. Cordioli, and F. Avallone, "Validation of high-fidelity numerical simulations of acoustic liners under grazing flow," in *AIAA AVIATION 2023 Forum*, 2021.

[21] F. Avallone and D. Casalino, "Acoustic-induced velocity in a multi-orifice acoustic liner grazed by a turbulent boundary layer," in *AIAA Aviation and Aeronautics Forum and Exposition, AIAA AVIATION Forum 2021*, American Institute of Aeronautics and Astronautics Inc, AIAA, 2021.

[22] P. Jaiswal and B. Ganapathisubramani, "Effects of porous substrates on the structure of turbulent boundary layers," *Journal of Fluid Mechanics*, vol. 980, p. A39, 2024.

[23] F. Scarano, M. C. Jacob, and E. R. Gowree, "Drag reduction by means of an array of staggered circular cavities at moderate reynolds numbers," *International Journal of Heat and Fluid Flow*, vol. 102, p. 109142, 2023.

[24] M. Kadivar, D. Tormey, and G. McGranaghan, "A review on turbulent flow over rough surfaces: Fundamentals and theories," *International Journal of Thermofluids*, vol. 10, p. 100077, 2021.

[25] J. Yu, M. Ruiz, and H. W. Kwan, "Validation of Goodrich perforate liner impedance model using NASA langley test data," in *14th AIAA/CEAS Aeroacoustics Conference (29th AIAA Aeroacoustics Conference)*, 2008.